Western University
Scholarship@Western

Paediatrics Publications | Paediatrics Department

11-1-2010

Feasibility and precision of cerebral blood flow and cerebrovascular reactivity MRI measurements using a computer-controlled gas delivery system in an anesthetised juvenile animal model

Jeff D. Winter
Hospital for Sick Children University of Toronto

Jorn Fierstra
University Health Network University of Toronto

Stephanie Dorner
University Health Network University of Toronto

Joseph A. Fisher
University Health Network University of Toronto

Keith S. Lawrence
Lawson Health Research Center, kstlawr@uwo.ca

See next page for additional authors

Follow this and additional works at: https://ir.lib.uwo.ca/paedpub

Citation of this paper:
Winter, Jeff D.; Fierstra, Jorn; Dorner, Stephanie; Fisher, Joseph A.; Lawrence, Keith S.; and Kassner, Andrea, "Feasibility and precision of cerebral blood flow and cerebrovascular reactivity MRI measurements using a computer-controlled gas delivery system in an anesthetised juvenile animal model" (2010). *Paediatrics Publications*. 1937.
https://ir.lib.uwo.ca/paedpub/1937

Authors
Jeff D. Winter, Jorn Fierstra, Stephanie Dorner, Joseph A. Fisher, Keith S. Lawrence, and Andrea Kassner

This article is available at Scholarship@Western: https://ir.lib.uwo.ca/paedpub/1937

Original Research

Feasibility and Precision of Cerebral Blood Flow and Cerebrovascular Reactivity MRI Measurements Using a Computer-Controlled Gas Delivery System in an Anesthetised Juvenile Animal Model

Jeff D. Winter, PhD,[1] Jorn Fierstra, MD,[2,3] Stephanie Dorner, RRT,[4] Joseph A. Fisher, MD,[5,6] Keith S. St. Lawrence, PhD,[7,8] and Andrea Kassner, PhD[1,9]*

Purpose: To demonstrate the feasibility and repeatability of cerebrovascular reactivity (CVR) imaging using a controlled CO_2 challenge in mechanically ventilated juvenile pigs.

Materials and Methods: Precise end-tidal partial pressure CO_2 (P_{ETCO_2}) control was achieved via a computer-controlled model-driven prospective end-tidal targeting (MPET) system integrated with mechanical ventilation using a custom-built secondary breathing circuit. Test-retest blood-oxygen level dependent (BOLD) CVR images were collected in nine juvenile pigs by quantifying the BOLD response to iso-oxic square-wave P_{ETCO_2} changes. For comparison, test-retest baseline arterial spin labeling (ASL) cerebral blood flow (CBF) images were collected. Repeatability was quantified using the intra-class correlation coefficient (ICC) and coefficient of variation (CV).

Results: The repeatability of the $PETCO_2$ (CV < 2%) step changes resulted in BOLD CVR ICC > 0.94 and CV < 6% for cortical brain regions, which was similar to ASL CBF repeatability (ICC > 0.96 and CV < 4%).

Conclusion: This study demonstrates the feasibility and precision of CVR imaging with an MPET CO_2 challenge in mechanically ventilated subjects using an animal model. Translation of this method into clinical imaging protocols may enable CVR imaging in young children with cerebrovascular disease who require general anesthesia.

Key Words: cerebrovascular reactivity; cerebral blood flow; arterial spin labeling; blood-oxygen level dependent; end-tidal CO2

J. Magn. Reson. Imaging 2010;32:1068–1075.

© 2010 Wiley-Liss, Inc.

CHILDHOOD CEREBROVASCULAR DISORDERS such as sickle cell disease, moyamoya, and cerebral arteriopathies have been identified as risk factors for stroke and are significant causes of mortality and long-term morbidity (1,2). Given that cerebral hemodynamic vulnerability is often associated with encroachment on vasodilatory reserve, a surrogate measure of regional cerebral blood flow (CBF) reserve would enhance the assessment and management of pediatric cerebrovascular disease. A potentially valuable measure is cerebrovascular reactivity (CVR), which is the quantification of the CBF response to a vasoactive stimulus (e.g., carbon dioxide). MRI measures of CVR have been used to identify hemodynamic compromise in adult patients (3–5), however, the use of MRI-based CVR measurements to study childhood cerebral vascular disease has been limited to children who were sufficiently cooperative to be studied awake and breathing on their own (6).

One key consideration in the implementation of CVR imaging in children is the respiratory challenge used to alter the arterial partial pressure of CO_2 ($PaCO_2$). Conventional methods of CO_2 manipulation include breath-holding, hyperventilation and inhalation of a fixed concentration of CO_2 balanced with medical air or oxygen. Although these methods do not require specialized equipment, they lack the ability to

[1]Department of Physiology and Experimental Medicine, The Hospital for Sick Children, Toronto, Ontario, Canada.
[2]Department of Medical Imaging, University Health Network, Toronto, Ontario, Canada.
[3]Department of Neurosurgery, University Health Network, Toronto, Ontario, Canada.
[4]Respiratory Therapy, University Health Network, Toronto, Ontario, Canada.
[5]Department of Anesthesiology, University Health Network, Toronto, Ontario, Canada.
[6]Department of Physiology, University of Toronto, Toronto, Ontario, Canada.
[7]Imaging Division, Lawson Health Institute, London, Ontario, Canada.
[8]Department of Medical Biophysics, University of Western Ontario, London, Ontario, Canada.
[9]Department of Medical Imaging, University of Toronto, Toronto, Ontario, Canada.

Contract grant sponsor: Ontario Research and Development Challenge Fund, The Hospital for Sick Children Research Institute Trainee Start-up Fund, Canada Research Chair Program.

*Address reprint requests to: A.K., Department of Medical Imaging, University of Toronto, Fitzgerald Building, 150 College Street, Toronto, Ontario M5S 3E2 Canada.
E-mail: andrea.kassner@utoronto.ca

Received December 11, 2009; Accepted April 8, 2010.
DOI 10.1002/jmri.22230
View this article online at wileyonlinelibrary.com.

© 2010 Wiley-Liss, Inc.

accurately target specific CO_2 levels. Moreover, the induced CO_2 changes are generally slow to implement, unpredictable in extent, and unstable over time. Improvements in the efficacy of CVR imaging have been achieved with recent implementation of computer-controlled manipulation of end-tidal partial pressure of CO_2 ($P_{ET}CO_2$) levels, including dynamic end-tidal forcing (DEF) (7) and model-driven prospective end-tidal targeting (MPET) (8). The MPET system is a relatively compact device that uses low gas flows and has the unique advantage that the $P_{ET}CO_2$ steps generated closely match $PaCO_2$ levels (9). However, this gas delivery method, originally implemented in spontaneously breathing adults, requires modification for use in very young patients (typically less than three years of age) who frequently require general anesthesia and mechanical ventilation for imaging procedures (10).

The purpose of the current study was to demonstrate the feasibility and repeatability of CVR imaging using an MPET system to provide a controlled cerebrovascular challenge in anesthetised juvenile pigs. We selected the juvenile pig for this purpose as the brain is similar to humans in terms of both cerebrovasculature (11) and gray-matter-to-white-matter ratio (12). Moreover, the physical size of the pig will enable easy translation of this computer-controlled MPET system to young children. For CVR imaging, blood oxygen level-dependent (BOLD) MRI was used to provide an indirect measure of the changes in CBF in response to $P_{ET}CO_2$ transitions. We assessed the short-term reproducibility of the BOLD CVR measures and compared the results with the short-term reproducibility of CBF estimates obtained using arterial spin labeling (ASL).

MATERIALS AND METHODS

This study was approved by our institutional animal care committee, and all procedures were conducted according to the Canadian Council on Animal Care. Imaging data were obtained from nine male Yorkshire pigs (one to three months old) with a median body weight of 10 kg (range = 5.2–25.8 kg) scanned as part of an ongoing study of normal swine brain development. Repeatability metrics were obtained from consecutive test and retest BOLD-CVR measurements separated in time by approximately four minutes; and, the repeatability of test-retest (separated in time by approximately two minutes) ASL-based CBF images was also assessed in a subset of seven pigs.

Animal Preparation

Anesthesia was induced with 0.2 mL/kg Akmezine (intramuscular) and switched to 3% isoflurane for intubation and animal preparation. A catheter was inserted into the ear vein for a constant delivery of intravenous anesthesia (22 mg/kg ketamine with 1 mg/kg midazolam). Pigs were transported to the MRI scanner and mechanically ventilated with an oxygen/medical air mixture. After the pig was stabilized on the ventilator, a bolus of 0.2 mg/kg pancuronium was delivered via the ear vein and infused at a constant rate of 1 mg/kg/hour for the duration of the experiment. Pigs were allowed to stabilize for at least 30 minutes prior to cerebrovascular imaging.

Computer-Controlled Gas Delivery System

The $P_{ET}CO_2$ and end-tidal partial pressure of O_2 ($P_{ET}O_2$) were controlled using an MPET system consisting of a sequential gas delivery breathing circuit in combination with an automated gas blender (RespirAct™, Thornhill Research Inc., Toronto, Canada). Slessarev et al (13) previously described and demonstrated this method in spontaneously breathing adult human subjects. Briefly, the RespirAct™ prospectively targets $P_{ET}CO_2$ and $P_{ET}O_2$ by adjusting the composition and flow rates of source gases based on the subject's CO_2 production and O_2 consumption. This fresh gas mixture is delivered to the subject by a sequential gas delivery breathing circuit, consisting of two one-way valves, one cross-over valve, an inspiratory and an expiratory reservoir. This breathing circuit directs the fresh gas mixture to the subject and ensures the balance of the subject's tidal volume is delivered from the expiratory reservoir via the cross-over valve (sequential rebreathing cycle). For the current study, we developed a secondary circuit to administer the gas output of the Respiract™ to the mechanically ventilated animals (Fig. 1). This secondary breathing circuit consisted of inspiratory and ventilator reservoirs encased in an air-tight polymethyl methacrylate box, which acts as an expiratory reservoir. The net effect of the circuit was to deliver the gases in a sequential rebreathing cycle, as described by Slessarev et al (13), in order to maintain $P_{ET}CO_2$ levels that are in close agreement with $PaCO_2$ (9).

Expired gases were continuously sampled from the endotracheal tube and the PCO_2 and PO_2 were measured using sensors within the RespirAct™ automated gas blender and recorded using customizable data acquisition software (LabView; National Instruments Corporation, Austin, TX, USA) that enabled automated identification of the breath-by-breath $P_{ET}CO_2$ and $P_{ET}O_2$. End-tidal selection from the PCO_2 waveforms was verified manually.

Anatomical MRI

MRI data were collected on a 1.5 T GE Signa MRI (General Electric Healthcare, Milwaukee, WI, USA) equipped with 40 mT/m gradients. Radiofrequency transmission was achieved with a body coil and an eight-channel receive-only head coil was used for radiofrequency detection. To isolate tissue regions, three-dimensional (3D) anatomical images were acquired with a high-resolution T1-weighted fast spoiled gradient-recalled echo sequence using the following imaging parameters: TE = 4.2 msec, TR = 8.46 msec, flip angle = 20°, field-of-view (FOV) = 180 mm, slab thickness = 180 mm, matrix size = 192 × 192 × 120.

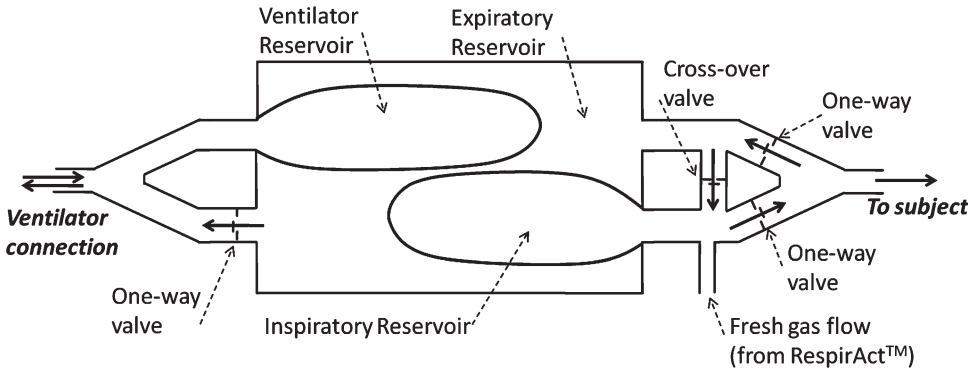

Figure 1. Schematic diagram of the secondary breathing system designed to incorporate sequential gas delivery and mechanical ventilation. The circuit was attached to the pig's endotracheal tube via a manifold that separates into inspiratory and expiratory branches, which are distinguished by the directionality of one-way low resistance valves. A conduit connects the two branches using a one-way cross-over valve with a resistance set greater than both of the one-way valves in the two branches. The breathing circuit functions as follows. During the expiratory phase, exhaled gases are directed through the expiratory reservoir (box) to the ventilator via the one-way valve on the manifold connected to the ventilator. And, the last portion of each exhaled breath remains within the expiratory reservoir. Fresh gases are continuously collected in the inspiratory reservoir from the RespirAct™. During the inspiratory phase, ventilator reservoir inflates, increasing pressure in the box, which forces fresh gases from the inspiratory reservoir and inlet into the subject. The fresh gas flow is set lower than the minute ventilation so that during the inspiratory phase, the inspiratory reservoir is completely depleted and collapses. Negative pressure in the inspiratory limb causes the cross-over valve to open, which then delivers the balance of the breath from the expiratory reservoir.

Blood-Oxygen Level Dependent (BOLD) CVR Imaging and Analysis

BOLD images were collected using a single-shot gradient-echo echo-planar imaging sequence during controlled cycling of the $P_{ET}CO_2$. Imaging parameters included: FOV = 160 mm, matrix size = 64 × 64, number of slices = 14–16, slice thickness = 4.5 mm, slice separation = 0.5 mm, TE = 35 msec and TR = 2 seconds. Square-wave $P_{ET}CO_2$ transitions, consisted of five steps of normocapnia ($P_{ET}CO_2$ = 40 mmHg for 60 seconds) separated by four steps of hypercapnia ($P_{ET}CO_2$ = 55 mmHg for 60 seconds) during BOLD imaging.

CVR post-processing was performed offline with FSL (FMRIB Software Library, http://www.fmrib.ox.ac.uk/fsl, Oxford University, UK) and in-house MatLab (MathWorks, Natick, MA, USA) scripts. BOLD images were spatially smoothed with a Gaussian kernel (full-width half-maximum [FWHM] = 5 mm), motion corrected and high-pass filtered using FEAT (FMRI Expert Analysis Tool, v 5.98, FMRIB). $P_{ET}CO_2$ and BOLD MRI time courses were matched by identifying shift of the $P_{ET}CO_2$ that generated the maximum correlation coefficient to the BOLD signal. This time delay is attributed to the time required for mixing and inhalation of fresh gases from the RespirAct™, the delayed physiological response, and the transition time of sampled gas from the endotracheal tube to the gas analyzers. Once in phase, CVR (% Δ BOLD signal/mmHg CO_2) was quantified on a pixel-by-pixel basis from the slope of the regression of % BOLD signal with $P_{ET}CO_2$. The temporal derivative of the $P_{ET}CO_2$ time series was also included in the model to remove the effect of small time shifts in the BOLD response.

ASL Acquisition and Analysis

Baseline CBF measurements were collected with $P_{ET}CO_2$ maintained at 40 mmHg by the MPET experimental setup described above for BOLD-CVR imaging. CBF was measured by collecting ASL data from six coronal slices through the pig's head using a single-shot gradient-echo spiral imaging sequence. The ASL method was based on flow-sensitive alternating inversion recovery technique, with a spin labeling pulse that alternated between slab-selection (39.6 mm) and global inversion (14). Static tissue water signal was suppressed using background suppression (15). The duration of the labeling period was defined by an arterial saturation pulse (35 mm in width) applied 850 msec after the spin labeling pulse. Prior to acquiring perfusion data, four proton-density (i.e., M_0) images were acquired for CBF quantification. A series of tag-control image pairs were collected at an inversion time (TI) = 1700 msec to generate a total of 64 perfusion-weighted (i.e., ΔM) images. Using a Look-Locker acquisition (16), we quantified the brain tissue R_1 relaxation rate ($R_{1\text{tissue}}$) by fitting a train of 11 low flip angle (20°) T_1-weighted images collected at TIs separated by 300 msec. All ASL images were acquired with the following imaging parameters: FOV = 160 mm, matrix size = 64 × 64, slice thickness = 5 mm, slice separation = 1 mm, TE = 4 msec and TR = 3.75 seconds.

All ASL post-processing was performed using scripts written in IDL (Interactive Data Language, Research Systems, Boulder, CO, USA) and MatLab. These post-processing steps included: generating the spiral images by interpolating the k-space data onto a Cartesian grid, performing the pair-wise subtraction of the complex "tag" and "control" images, and

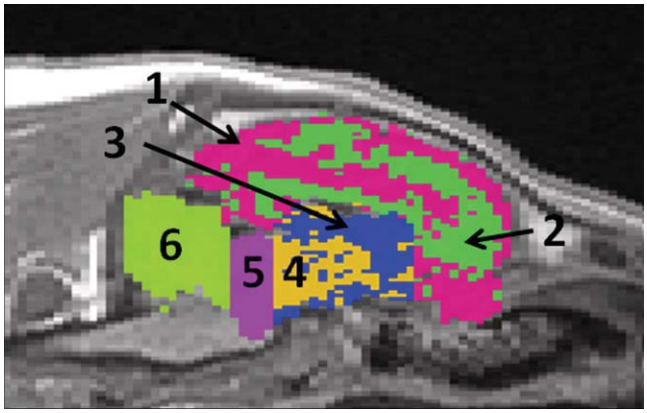

Figure 2. Saggital T1-weighted anatomical MRI with tissue regions-of-interest overlaid, including 1: cortical gray matter (GM); 2: cortical white matter (WM); 3: deep GM; 4: deep WM; 5: mesacephalon; and 6: cerebellum. The image was cropped to isolate the brain. [Color figure can be viewed in the online issue, which is available at wileyonlinelibrary.com.]

generating the average ΔM images. The CBF values were obtained using the following equation (15,17):

$$\frac{\Delta M}{M_0} = -\frac{2\alpha}{\lambda} \cdot CBF \cdot e^{-R_{1a} \cdot TI} \times \left[\frac{(1 - e^{-\Delta R_1 \cdot (TI - \tau)})}{\Delta R_1} + (\tau + d - TI) \right] \quad [1]$$

where ΔM is the magnitude of the perfusion-weighted image, M_0 is the equilibrium MR signal, α is set to 0.85 to account for background-suppression related signal losses, λ (0.9 mL/g) is the partition coefficient of water, R_{1a} (0.8 seconds^{-1}) is the arterial water longitudinal relaxation rate at 1.5 T (18), $\Delta R_1 = R_{1a} - R_{1tissue}$, TI is the TI adjusted on a slice-by-slice basis, τ (1130 msec) is the tissue transit time (17), and d is the time between the inversion pulse and the arterial saturation pulse. Pixels with CBF greater than 200 mL/100 g/minute were considered vascular and removed from both trials.

Brain Tissue Segmentation

The 3D anatomical images were segmented into six tissue regions using both automatic (FMRIB Automated Segmentation Tool, FAST) (19) and follow-up manual segmentation. Regions identified include cortical gray matter (GM), cortical white matter (WM), deep GM, deep WM, mesencephalon, and cerebellum (Fig. 2). BOLD CVR and CBF images were transformed to the anatomical images via low resolution T1-weighted images collected at the same slice locations as the BOLD and ASL datasets (FMRIB Linear Image Registration Tool, FLIRT) (20). Mean CVR and CBF values for test-retest acquisitions were extracted for each tissue region. CBF measures were not available for the mesencephalon and cerebellum because of the limited spatial coverage in the ASL acquisition.

Statistical Analysis

To assess the repeatability of the CO_2 transitions, we calculated the coefficient of variation (CV = SD/mean $\times$ 100%) for the $P_{ET}CO_2$ at each square-wave step. Between-trial bias of CVR estimates and limits of agreement were assessed using Bland-Altman analysis. To quantify repeatability, we performed a random effects variance components analysis to compute the intra-class correlation coefficient (ICC) (21) for each region separately for both the CVR and CBF data. We also computed repeatability of the CVR and CBF measurements using the CV for comparison with previous studies. Statistical analyses were performed with SPSS version 11 (SPSS Inc., Chicago, IL, USA).

RESULTS

The measured $P_{ET}CO_2$ and $P_{ET}O_2$ matched the targeted $P_{ET}CO_2$ and $P_{ET}O_2$ levels in the end-tidal sequence delivered by the RespirAct™, although a small spike was observed at the start of each transition to hypercapnia (Fig. 3). Table 1 presents the measured $P_{ET}CO_2$ levels achieved for all stages of the BOLD CVR experiments averaged across all subjects. The measured normocapnia $P_{ET}CO_2$ levels of 41.1 ± 2.6 mmHg (mean ± SD), averaged over all subjects and stages closely matched our target level of 40

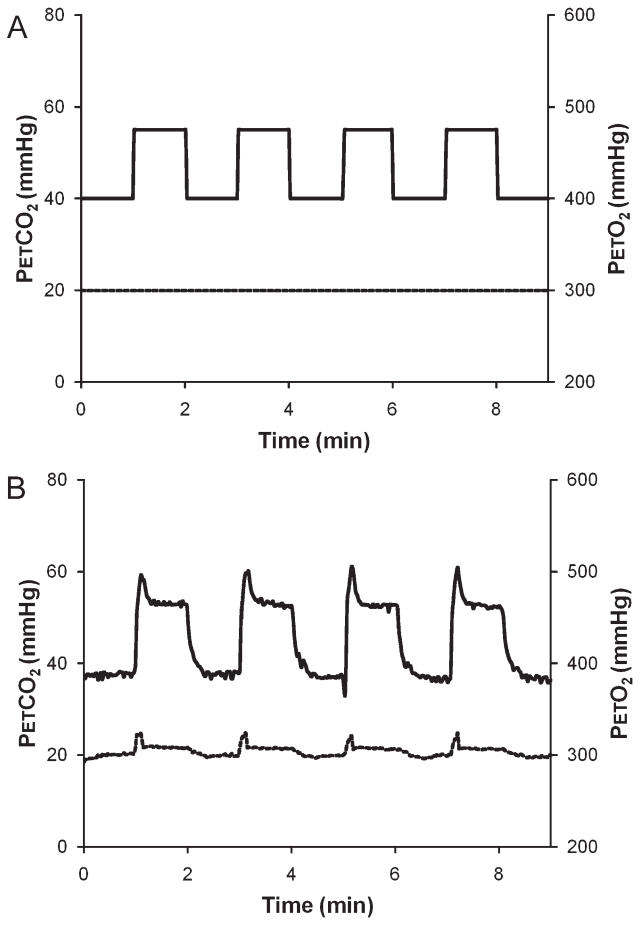

Figure 3. Targeted (**a**) and measured (**b**) $P_{ET}CO_2$ (solid line) and $P_{ET}O_2$ (dashed line) levels for an end-tidal sequence delivered by the RespirAct™ system during the BOLD MRI acquisition in a two-month-old pig. The control of $P_{ET}O_2$ was maintained despite large changes in $P_{ET}CO_2$.

Table 1
Mean $P_{ET}CO_2$ Levels Achieved for Each BOLD CVR Trial*

Stage	$P_{ET}CO_2$ (mmHg) Trial 1	Trial 2	CV (%)
Normocapnia 1	40.6 ± 2.0	40.9 ± 2.0	1.8 ± 0.7
Hypercapnia 1	54.7 ± 1.8	55.1 ± 1.8	1.1 ± 0.7
Normocapnia 2	41.1 ± 2.2	41.4 ± 2.2	1.9 ± 0.6
Hypercapnia 2	55.2 ± 1.9	55.5 ± 1.9	1.0 ± 0.7
Normocapnia 3	41.5 ± 2.7	41.8 ± 2.8	1.5 ± 0.9
Hypercapnia 3	55.4 ± 2.1	55.6 ± 2.1	1.0 ± 0.6
Normocapnia 4	41.9 ± 2.9	42.3 ± 2.9	1.6 ± 1.1
Hypercapnia 4	55.5 ± 2.2	55.6 ± 2.2	1.0 ± 0.9

*Mean $P_{ET}CO_2$ and the mean between-trial coefficient of variation (CV) values averaged across all subjects for each of the eight stages in the BOLD CVR imaging protocol. Data are presented mean ± SD.

mmHg. Similarly, the targeted hypercapnia $P_{ET}CO_2$ level of 55 mmHg was also closely matched by the measured values (56.2 ± 2.7 mmHg). Excellent test-retest repeatability existed for each stage in the square wave $P_{ET}CO_2$ cycle (CV < 2 %, Table 1). In addition to well-defined square-wave transitions, baseline values were restored with high reliability, showing a small positive drift of only 1.3 mmHg for the normocapnia steps and 0.6 mmHg for the hypercapnia steps. Good control of $P_{ET}O_2$ was maintained during the $P_{ET}O_2$ transitions (Fig. 3b). For the ASL acquisition, we targeted a constant $P_{ET}CO_2$ of 40 mmHg for both trials. Mean $P_{ET}CO_2$ levels in the ASL acquisition, averaged over all subjects, were 41.2 ± 1.6 mmHg for the first trial and 41.0 ± 1.5 mmHg for the second trial, with a between-trial CV of 1.1 ± 0.7 %.

The BOLD signal response closely followed the changes in the $P_{ET}CO_2$ values, after temporal matching of the two signals (Fig. 4). Representative test-retest BOLD CVR images and corresponding test-retest baseline ASL CBF images collected from the same two-month old pig are shown in Figure 5. These images show the consistency the CVR and CBF values between the two trials. Figure 6 presents the BOLD-CVR repeatability assessment performed using Bland-Altman analysis for all regions investigated. The mean test-retest difference for cortical GM was 0.0023%/mmHg, with ± 0.0086%/mmHg (±1.96 × SD) limits of agreement and the mean cortical WM difference was 0.0021%/mmHg, with ± 0.0081%/mmHg limits of agreement. Mean test-retest BOLD-CVR differences in the deep GM, deep WM and mesencephalon regions were similar to those observed in the cortical regions, but, the limits of agreement were greater. The cerebellum showed similar mean differences and limits of agreement to the cortical regions. Table 2 provides the ICC and CV repeatability measures for the BOLD CVR results for all six regions interrogated. The cortical regions and cerebellum exhibited excellent BOLD CVR repeatability (ICC > 0.94), and all other regions exhibited good to excellent repeatability (ICC > 0.75).

The global CBF, across all subjects, trials, and regions was 54.1 ± 12.5 mL/100 g/minute (mean ±

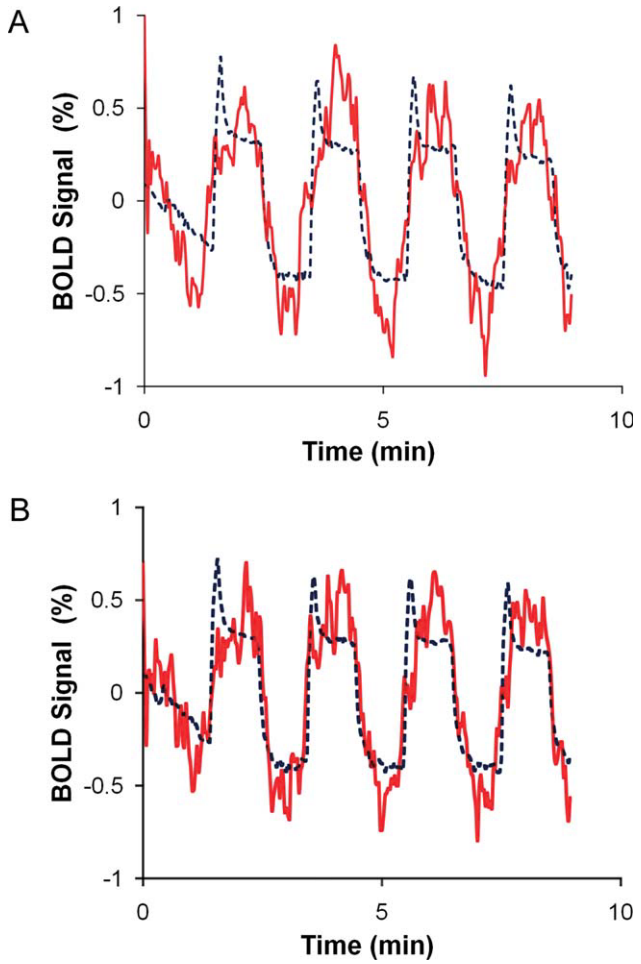

Figure 4. Representative test (**a**) and retest (**b**) BOLD signal intensity time series (solid line) averaged across all brain tissue, with the modelled $P_{ET}CO_2$ time course (dashed line) overlaid.

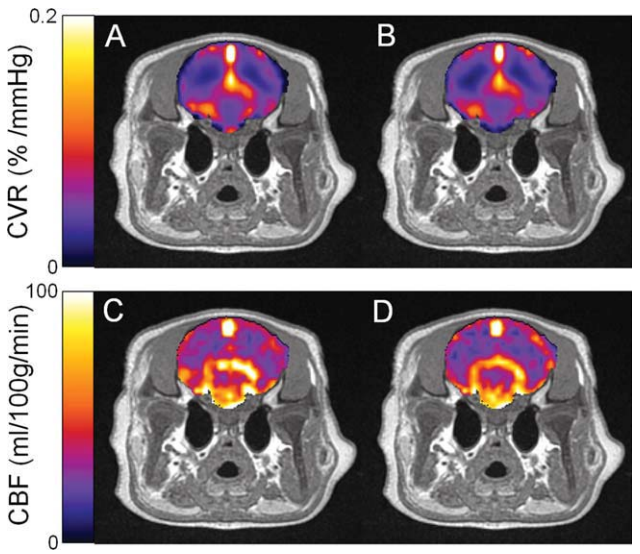

Figure 5. Representative BOLD cerebrovascular reactivity (CVR) images for trial 1 (**a**) and trial 2 (**b**) along with corresponding ASL CBF images for trial 1 (**c**) and trial 2 (**d**) collected from a two-month old pig. The CVR and CBF images were registered to the anatomical images and all non-brain-tissue pixels were removed. All images were cropped to highlight the brain.

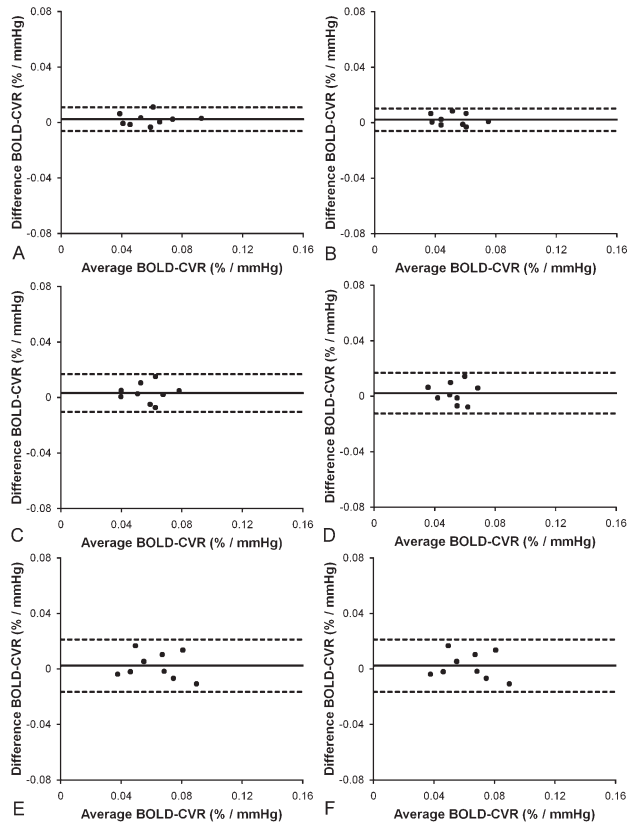

Figure 6. Bland-Altmann plots for test-retest BOLD-CVR measurements (two minutes apart) demonstrating repeatability for regions of cortical GM (**a**), cortical WM (**b**), deep GM (**c**), deep WM (**d**), mesencephalon (**e**), and cerebellum (**f**). The mean BOLD-CVR difference is represented by a solid line and the 95% confidence intervals are displayed with a dashed line.

SD) determined using the measured $R_{1tissue}$ (0.85 ± 0.01 second^{-1}). Regional CBF levels are provided in Table 3 along with the reliability measures. Similar to the BOLD CVR, between-trial ICC and CV results for ASL measures of CBF also exhibited excellent reproducibility for the cortical GM and WM regions (ICC > 0.95) as well as the deep GM and WM regions (ICC > 0.80).

DISCUSSION

Advances in computer-controlled gas delivery systems have improved imaging-based CVR quantification by providing rapid and reproducible changes in $P_{ET}CO_2$ while maintaining $P_{ET}O_2$ levels (7,8). These systems have considerable promise for the noninvasive assessment of CVR in adults and older children with cerebrovascular disease; however, there is a need to integrate gas delivery with mechanical ventilation for younger children who often require general anesthesia for imaging procedures. In the current study, we demonstrated the first application of an MRI-compatible computer-controlled CO_2 gas delivery system in anaesthetized and ventilated animals for the purpose of obtaining high-quality BOLD CVR images. To our knowledge, this is the first report to provide quantitative values of BOLD CVR measurements in an animal model and the first to report short-term reproducibility of the method. In the absence of previous literature for comparison, we evaluated BOLD CVR reliability against an established cerebrovascular imaging technique, ASL, which has been validated in newborn pigs (17). In this study we found excellent repeatability for ASL CBF measures for all regions investigated. Similarly, BOLD CVR measurement repeatability was classified as excellent in the cortical regions (ICC > 0.94) and good to excellent (ICC > 0.75) for all other regions. BOLD CVR repeatability observed in the current study (CV < 9 %, for all brain regions) was superior to a recent human study that employed a 10 % fixed CO_2 inhalation to investigate short-term reproducibility (GM CV = 23.8 % and WM CV = 24.7 %) (22). We infer that the repeatability of BOLD CVR measures has improved in the current study due to a combination of reduced subject motion (anesthesia) and controlled $P_{ET}CO_2$ transitions.

This is also the first study to report the implementation of MPET with mechanical ventilation. This was achieved with a custom-built secondary breathing circuit that incorporated sequential gas delivery with partial rebreathing of exhaled gases. Sequential gas delivery enables accurate prospective targeting of $P_{ET}CO_2$ and $P_{ET}O_2$ levels and ensures that $P_{ET}CO_2$ transitions agree with targeted $PaCO_2$ levels (9). The secondary circuit retained the rapid transitions and accurate end-tidal targeting of the original method (13), which minimizes issues regarding BOLD signal drift; and, the ability to clamp $P_{ET}O_2$ independently of changes in $P_{ET}CO_2$ removes the influence of arterial O_2 changes on the BOLD signal (8).

An alternative approach to generate controlled CO_2 transitions is DEF of CO_2, which was previously utilized in young pigs under anesthetic (23); however

Table 2
Mean Values and Coefficients of Variation of Test-Retest BOLD CVR Results*

Region	BOLD CVR (%/mmHg), mean ± SD		CV (%) between-trial, mean ± SD	ICC between-trial, mean [95% CI]
	Trial 1	Trial 2		
Cortical GM	0.060 ± 0.017	0.058 ± 0.017	4.6 ± 1.5	0.96 [0.85 0.99]
Cortical WM	0.053 ± 0.012	0.051 ± 0.013	5.0 ± 1.5	0.94 [0.77, 0.99]
Deep GM	0.059 ± 0.011	0.055 ± 0.013	7.0 ± 2.1	0.85 [0.50 0.96]
Deep WM	0.054 ± 0.004	0.052 ± 0.011	8.1 ± 1.9	0.76 [0.28, 0.94]
Mesencephalon	0.064 ± 0.017	0.062 ± 0.019	9.0 ± 2.2	0.86 [0.53, 0.97]
Cerebellum	0.076 ± 0.025	0.075 ± 0.027	4.4 ± 0.6	0.98 [0.92 0.99]

*N = 9. CV = coefficient of variation, ICC = intraclass correlation coefficient, CI = confidence interval.

Table 3
Mean Values and Coefficients of Variation of Test-Retest ASL-CBF Results*

Region	CBF (mL·100 g^{-1}·$minute^{-1}$), mean ± SD		CV (%) between-trial, mean ± SD	ICC between-trial, mean [95% CI]
	Trial 1	Trial 2		
Cortical GM	53 ± 9	52 ± 10	3.1 ± 3.5	0.95 [0.76 0.99]
Cortical WM	41 ± 5	40 ± 5	2.0 ± 1.8	0.95 [0.77, 0.99]
Deep GM	69 ± 7	66 ± 6	2.9 ± 3.2	0.81 [0.31 0.97]
Deep WM	56 ± 8	54 ± 8	3.7 ± 4.2	0.88 [0.51, 0.98]

*$N = 7$. CV = coefficient of variation, ICC= intraclass correlation coefficient, CI = confidence interval.

these animals were free-breathing. Control of end-tidal gases using DEF has not been described in ventilated subjects. DEF generally involves a closed feedback system with sophisticated prediction-correction algorithms controlling the subject's $P_{ET}CO_2$ levels. This method is capable of generating rapid CO_2 transitions within the MRI environment (7). The main limitation of this method relates to its implementation, which is generally complex, expensive, and requires large gas stores to deliver the high gas flow levels required to attain peak inspiratory flows (7). A relatively compact DEF system has recently been described (24) for use in studies of ventilatory response, however its use in the MR environment and with ventilated subjects has not yet been demonstrated. The caveat is that end-tidal forcing systems have in common the use of pure CO_2, O_2, and N_2 as source gases, raising the risk of sudden anoxia and death should the O_2 gas flow inadvertently fail, even for a few seconds. The Respiract™ mitigates this risk by not using anoxic source gases, which is particularly relevant for future clinical applications involving children.

The square-wave $P_{ET}CO_2$ transitions generated in the current study were in agreement with targeted levels. Each step in the cycle also provided excellent repeatability (between-trial CV < 2 %), although we did observe a $P_{ET}CO_2$ "spike" following each transition to hypercapnia and a small drift in the baseline $P_{ET}CO_2$ levels across all transitions. The initial $P_{ET}CO_2$ spikes are most likely related to the mixing of inspired gases within the lungs during each transition to hypercapnia, and may be more pronounced in the current study, compared with previous human studies (13), owing to direct sampling from the endotracheal tube. The $P_{ET}CO_2$ drift may be attributed to the large magnitude of the transitions (~15 mmHg) as well as to the short stage duration for each transition (60 seconds). The intervals may not have been sufficient to allow the $P_{ET}CO_2$ levels to return to baseline (40 mmHg). As the above-mentioned CO_2 drift exhibited a similar pattern for test and retest experiments, between-trial repeatability for each individual step was not greatly affected. Consistently and precisely targeted iso-oxic $P_{ET}CO_2$ transitions may also benefit studies of the physiology of brain vasculature, animal models of cerebrovascular disease, or neuropharmacology of drugs as well as animal studies investigating the hemodynamic response to functional stimuli (25).

The magnitude of the BOLD response to $P_{ET}CO_2$ changes acquired in this study in the juvenile pig (cortical GM = 0.058%/mmHg) were approximately half of that reported in awake, spontaneously breathing, human subjects (GM BOLD CVR = 0.12 ± 0.03%/mmHg on a 1.5 T scanner with a similar echo time) (26). The lower BOLD CVR values in the current study may reflect species differences in cerebrovascular function, age-related developmental effects, and/or anesthetic effects. Previous work in rats demonstrated a significant attenuation of the BOLD response to CO_2 inhalation in the anaesthetized state compared to awake (27).

The anesthetics used in the study may have also impacted CBF measurements, as previous swine studies demonstrated that ketamine administered either alone or in combination with midazolam can decrease CBF, when compared with a fentanyl and nitrous oxide mixture (28,29). The CBF estimates in the current study are similar to previous reports, including a positron emission tomography (PET) study in the one-year old Gottengin minipig that found whole brain CBF of 49.0 ± 6.7 mL·100 g^{-1}·$minute^{-1}$ (30) and a microsphere study performed in the Yucatan minipig, with a global CBF of 63.4 ± 12.0 in four-week old pigs and 60.8 ± 12.1 in 10-week old pigs (31). However, our CBF measurements were greater than those reported in a previous PET study performed in two- to three-month old domestic pigs, which found whole brain CBF levels of 27 ± 5 mL·100 g^{-1}·$minute^{-1}$ (32). Our results were lower than an ASL study performed in newborn domestic pigs, which found greater CBF in the GM (73 mL·100 g^{-1}·$minute^{-1}$) and WM (60 mL·100 g^{-1}·$minute^{-1}$ regions (17) compared with the current study. Variability of literature CBF estimates may be related to breed, anesthetics and measurement technique.

In conclusion, this study provides the first demonstration of computer-controlled targeting of $P_{ET}CO_2$ and $P_{ET}O_2$ integrated with mechanical ventilation within the MRI environment. This study in 5.2 kg to 25.8 kg pigs was scaled to test the practicality for use in small children. We observed excellent trial repeatability for the square-wave CO_2 stimulus, as well as the BOLD measurements of CVR. Translation of this method of gas delivery for clinical pediatric studies would, for the first time, enable CVR tests of small children and other patients who require anesthesia for compliance during imaging procedures. We also anticipate that improved experimental manipulation of CO_2 levels in animal studies may benefit the study of cerebrovascular development, function, pathology, or pharmacological agents.

REFERENCES

1. Lynch JK, Hirtz DG, DeVeber G, Nelson KB. Report of the National Institute of Neurological Disorders and Stroke workshop on perinatal and childhood stroke. Pediatrics 2002;109:116–123.
2. Jordan LC. Stroke in childhood. Neurologist 2006;12:94–102.
3. Mandell DM, Han JS, Poublanc J, et al. Mapping cerebrovascular reactivity using blood oxygen level-dependent MRI in Patients with arterial steno-occlusive disease: comparison with arterial spin labeling MRI. Stroke 2008;39:2021–2028.
4. Ziyeh S, Rick J, Reinhard M, Hetzel A, Mader I, Speck O. Blood oxygen level-dependent MRI of cerebral CO2 reactivity in severe carotid stenosis and occlusion. Stroke 2005;36:751–756.
5. Han JS, Mandell DM, Poublanc J, et al. BOLD-MRI cerebrovascular reactivity findings in cocaine-induced cerebral vasculitis. Nat Clin Pract Neurol 2008;4:628–632.
6. Mikulis DJ, Krolczyk G, Desal H, et al. Preoperative and postoperative mapping of cerebrovascular reactivity in moyamoya disease by using blood oxygen level-dependent magnetic resonance imaging. J neurosurg 2005;103:347–355.
7. Wise RG, Pattinson KT, Bulte DP, et al. Dynamic forcing of end-tidal carbon dioxide and oxygen applied to functional magnetic resonance imaging. J Cereb Blood Flow Metab 2007;27: 1521–1532.
8. Prisman E, Slessarev M, Han J, et al. Comparison of the effects of independently-controlled end-tidal PCO(2) and PO(2) on blood oxygen level-dependent (BOLD) MRI. J Magn Reson Imaging 2008;27:185–191.
9. Ito S, Mardimae A, Han J, et al. Non-invasive prospective targeting of arterial P(CO2) in subjects at rest. J Physiol 2008;586(Pt 15):3675–3682.
10. Lemaire C, Moran GR, Swan H. Impact of audio/visual systems on pediatric sedation in magnetic resonance imaging. J Magn Reson Imaging 2009;30:649–655.
11. Imai H, Konno K, Nakamura M, et al. A new model of focal cerebral ischemia in the miniature pig. J Neurosurg 2006;104(2 Suppl):123–132.
12. Dobbing J. The later growth of the brain and its vulnerability. Pediatrics 1974;53:2–6.
13. Slessarev M, Han J, Mardimae A, et al. Prospective targeting and control of end-tidal CO2 and O2 concentrations. J Physiol 2007; 581(Pt 3):1207–1219.
14. St Lawrence KS, Frank JA, Bandettini PA, Ye FQ. Noise reduction in multi-slice arterial spin tagging imaging. Magn Reson Med 2005;53:735–738.
15. Ye FQ, Frank JA, Weinberger DR, McLaughlin AC. Noise reduction in 3D perfusion imaging by attenuating the static signal in arterial spin tagging (ASSIST). Magn Reson Med 2000;44:92–100.
16. St Lawrence KS, Ye FQ, Lewis BK, Weinberger DR, Frank JA, McLaughlin AC. Effects of indomethacin on cerebral blood flow at rest and during hypercapnia: an arterial spin tagging study in humans. J Magn Reson Imaging 2002;15:628–635.
17. Koziak AM, Winter J, Lee TY, Thompson RT, St Lawrence KS. Validation study of a pulsed arterial spin labeling technique by comparison to perfusion computed tomography. Magn Resone Imaging 2008;26:543–553.
18. Ye FQ, Mattay VS, Jezzard P, Frank JA, Weinberger DR, McLaughlin AC. Correction for vascular artifacts in cerebral blood flow values measured by using arterial spin tagging techniques. Magn Reson Med 1997;37:226–235.
19. Zhang Y, Brady M, Smith S. Segmentation of brain MR images through a hidden Markov random field model and the expectation-maximization algorithm. IEEE Trans Med Imaging 2001;20: 45–57.
20. Jenkinson M, Smith S. A global optimisation method for robust affine registration of brain images. Med Image Anal 2001;5: 143–156.
21. Shrout PE, Fleiss JL. Intraclass correlations: uses in assessing rater reliability. Psychol Bull 1979;86:420–428.
22. Goode SD, Krishan S, Alexakis C, Mahajan R, Auer DP. Precision of cerebrovascular reactivity assessment with use of different quantification methods for hypercapnia functional MR imaging. AJNR Am J Neuroradiol 2009;30:972–977.
23. Wolsink JG, Berkenbosch A, DeGoede J, Olievier CN. Ventilatory sensitivities of peripheral and central chemoreceptors of young piglets to inhalation of CO2 in air. Pediatr Res 1991;30:491–495.
24. Koehle MS, Giles LV, Curtis AN, Walsh ML, White MD. Performance of a compact end-tidal forcing system. Respir Physiol Neurobiol 2009;167:155–161.
25. Zappe AC, Uludag K, Logothetis NK. Direct measurement of oxygen extraction with fMRI using 6% CO2 inhalation. Magn Reson Imaging 2008;26:961–967.
26. Mandell DM, Han JS, Poublanc J, et al. Selective reduction of blood flow to white matter during hypercapnia corresponds with leukoaraiosis. Stroke 2008;39:1993–1998.
27. Sicard K, Shen Q, Brevard ME, et al. Regional cerebral blood flow and BOLD responses in conscious and anesthetized rats under basal and hypercapnic conditions: implications for functional MRI studies. J Cereb Blood Flow Metab 2003;23:472–481.
28. Akeson J, Bjorkman S, Messeter K, Rosen I. Low-dose midazolam antagonizes cerebral metabolic stimulation by ketamine in the pig. Acta anaesthesiol Scand 1993;37:525–531.
29. Bjorkman S, Akeson J, Nilsson F, Messeter K, Roth B. Ketamine and midazolam decrease cerebral blood flow and consequently their own rate of transport to the brain: an application of mass balance pharmacokinetics with a changing regional blood flow. J Pharmacokinet Biopharm 1992;20:637–652.
30. Andersen F, Watanabe H, Bjarkam C, Danielsen EH, Cumming P. Pig brain stereotaxic standard space: mapping of cerebral blood flow normative values and effect of MPTP-lesioning. Brain Res Bull 2005;66:17–29.
31. Nomura F, Forbess JM, Jonas RA, et al. Influence of age on cerebral recovery after deep hypothermic circulatory arrest in piglets. Ann Thorac Surg 1996;62:115–122.
32. Mortberg E, Cumming P, Wiklund L, Rubertsson S. Cerebral metabolic rate of oxygen (CMRO2) in pig brain determined by PET after resuscitation from cardiac arrest. Resuscitation 2009;80: 701–706.